Ibn Al-Haitham Journal for Pure and Applied Sciences
Journal homepage: jih.uobaghdad.edu.iq
PISSN: 1609-4042, EISSN: 2521-3407
IHJPAS. 2026; 39(1)

Investigating the Influence of Cadmium Doping on the Electrical and Structural Properties of $Pb_{1-x}Cd_xBa_2Ca_2Cu_3O_{9+\delta}$ Superconductor

Hasan M. Ibrahim[1*], Muayed K. Ibrahim[2] and Kareem A. Jasim[3]

[1,2] Department of Energy Engineering, College of Engineering, University of Baghdad, Baghdad, Iraq
[3]Department of Physics, College of Education for Pure Science (Ibn Al-Haitham), University of Baghdad, Baghdad, Iraq
*Corresponding Author

Received: 27/January/2025
Accepted: 13/May/2025
Published: 20/January/2026
doi.org/10.30526/39.1.4124

Abstract

The superconducting compound ($Pb_{1-x}Cd_xBa_2Ca_2Cu_3O_{9+\delta}$) was prepared using the solid- state reaction (SSR) method as it is the most common method in the preparation of superconducting compounds, where the study was carried out at addition weights (x=0,0.15) to observe the effect of replacing lead with cadmium and the effect of this replacement on both the characteristics and behavior of the samples in terms of electrical resistance and critical temperature, where all samples displayed superconducting behavior. In this research, both the critical temperature of the compound and the dielectric properties of the compound (imaginary dielectric constant, real dielectric constant, alternating electrical conductivity, and loss tangent) were investigated as a function of frequency from the range (200 KHz-1 MHz) at room temperature, and the atomic force microscope (AFM) was also used to know the surface topography and surface roughness. The results of the atomic force microscope examination showed exceptional consistency and homogeneity of the processing flexure as a result of the chemical reaction between the raw materials where the grains were bonded to each other, and the temperatures were monitored at zero, resistivity was observed at $Tc_{(offset)}$ (147.3,146.9) K and $Tc_{(onset)}$ (200.25,198.92) K for both the addition ratio of (x=0,0.15), and the examination also showed that the surface roughness was medium. The results of the dielectric constant of the samples showed a change in the values of the real and imaginary dielectric constant, dielectric loss, and conductivity with the change of frequency magnitude from (200 KHz-1 MHz) for all samples used.

Keywords: Alternating electrical conductivity, Superconductivity, Dielectric properties, Imaginary dielectric constant, Electrical resistivity.

1. Introduction

Bednorz and Muller discovered superconductivity in the La-Ba-Cu-O system in 1986, which sparked research into copper oxide-based high-temperature superconductors known as high-temperature superconductors (HTS). Since then, scientists have created several hundred chemically different copper superconductors[1]. The discovery of superconductivity is attributed to the Dutch scientist Heike Kamerlingh Onnes in 1911. Onnes was studying the electrical resistance of some metals at very low temperatures to determine whether their resistance would continue to decrease linearly with temperature or remain constant. During his study, he observed a change in the resistance of mercury when cooled with liquid helium, and at 4.2 K the resistance suddenly disappeared[2]. In 1986, superconductivity entered a new phase with the discovery of some ceramic materials with a superconducting temperature above 90 K, known as high-temperature superconductors. This discovery was significant because it allowed the use of liquid nitrogen for cooling[3-5] at a temperature of 77 K, which is readily available and inexpensive[6,7].

The discovery of these materials has facilitated many experiments and applications, and research continues to find superconducting materials with higher critical temperatures to make applications more accessible. High-temperature superconducting ceramic compounds are characterized by the presence of one or more layers of copper oxide[8]. There is much interest in superconducting compounds with the chemical formula ($PbBa_2Can-1CunO_2n+2+\delta$) (n = 1, 2, 3-8, where n is the number of Cu-O layers), and the phases of this series have a high transition temperature (Tc), and the transition temperature increases as the number of Cu-O layers in the compound increases [9]. Some polycrystalline lead-based compounds have a perovskite structure of the unit cell[10]. The structure of lead-based superconductors is the same as that of single-layer CuO superconductors, with very few oxygen atoms bonded to the lead (Pb-O) layer, and the arrangement of the lead element is likely to vary greatly depending on the preparation method and conditions [11,12]. Different numbers of homogeneous Cu-O layers are responsible for high-temperature superconductivity [13,14]. Partial substitution of some chemical elements with positive valence by other chemical elements leads to high-phase superconducting phases (Pb-1223), which improves the properties of the compound, such as critical current density [15–17]. In this research, some physical properties of the superconducting compound ($Pb1-xCdxBa_2Ca_2Cu_3O_9+\delta$) have been studied, including the study of the structural properties to obtain the type of compound as well as the determination of the transition temperature using the continuous electrical conductivity. Superconductors are widely used in both engineering and medicine. The dielectric qualities of non-conducting materials can be used to explain how materials can interact with electric fields. Important features include the capture and storage of electrical potential energy in the form of polarization within the dielectric material, as well as the fractional dissipation of energy when the dielectric field is eliminated [9,10]. As these have applications in lasers that require special operation, magnetic resonance imaging, and radiology diagn ostics, it is important to establish the dielectric properties and electrical conductivity of these commercial materials [10].

2. Materials and Methods

The $Pb1-xCdxBa_2Ca2Cu_3O_9+\delta$ was prepared by the solid-state reaction process[18-20] utilizing high-purity oxides (lead oxide, copper oxide, calcium oxide, barium oxide, cadmium oxide) depending on their molecular weights [21,22] used according to the following chemical **Equation 1**:

$$(1-X)\ PbO + (X)\ CdO + 2BaO + 2CaO + 3CuO \rightarrow Pb1-xCdxBa_2Ca2Cu_3O9+\delta \quad \textbf{(1)}$$

The mixing and grinding were carried out with a manual garnet mortar to achieve smooth powders with a high level of homogeneity. This operation took one hour. The models were then shaped into cylindrical discs using a mould with a diameter of 1.5 cm and a thickness of 0.63 cm and a hydraulic press with a pressure of 7 tons for 2 minutes. A bi-directional axial compression mechanism was used to achieve the best and highest density value. The models were sintered at 850°C for 64 hours under atmospheric pressure at a heating rate of 5°C/min and cooled to room temperature at the same rate. The sintering process aims to obtain cohesive samples and to ensure optimal diffusion between the atoms. Atomic Force Microscopy (AFM) is a high-resolution scanning microscopy technique with resolution down to fractions of a nanometer. AFM enables the acquisition of three-dimensional topographic pictures of the investigated sample. It offers 2D and 3D images with a size of 3000 x 3000 nm and high resolution, illustrating details of surface topography, grain size, the total number of grains in the sample, and height. This method is used to measure the average diameter and surface morphology of the sample grains. The electrical resistivity (ρ) of the samples as a function of temperature was measured using the DC resistivity approach using four probes to validate the superconducting state.

To identify the dielectric characteristics involving dielectric constant (real dielectric constant (ἐ), imaginary dielectric constant (ἔ), loss tangent (tanδ), and alternating electrical conductivity (σ), it was achieved by the calculation of capacitance (C) and conductivity (G) using LCR impedance

device (4294A Precision Impedance Analyzer), where this device has a frequency range (40 Hz - 110 MHz), profiling and frequency ranges (200 KHz-1 MHz) and by the following relationships[23].

$$\dot{\varepsilon}=Cd/A\epsilon_o \quad (2)$$

$$\ddot{\varepsilon}=Gd/2\pi\rho\epsilon_o \quad (3)$$

$$\tan\delta=\ddot{\varepsilon}/\dot{\varepsilon} \quad (4)$$

$$\sigma=2\pi f^*\varepsilon_o^*\ddot{\varepsilon} \quad (5)$$

3. Results

3.1.AFM Measurement

The surface roughness of two samples was characterized using Atomic Force Microscopy (AFM) in accordance with ISO 25178 standards, with **Figures 1** and **2** illustrating the resulting 2D and 3D shapes. Sample 1 (x=0) had a root mean square height (Sq) of 351.7 nm, an arithmetic mean height (Sa) of 279.6 nm, and a maximum height (Sz) of 2527 nm, which showed that there were significant vertical variations. Its surface morphology was peak-dominated with positive skewness (Ssk = 0.1411$), high kurtosis (Sku = 3.228$), a material ratio (Smr) of 25.30%, and a void volume (Vv) of 453.5 nm³/nm³. Conversely, Sample 2 exhibited a slightly higher arithmetic mean height ($Sa = 285.8 nm) but a lower maximum height (S_z = 2163nm), with a texture characterized by a negative skewness (S_{sk} = -0.1129), lower kurtosis (S_{ku} = 2.664), a higher material ratio (S_{mr} = 54.73$), a void volume ($V_v$) of 479.9 nm³/nm³, an autocorrelation length (S_{al}) of 1226 nm, and gentler slope variations (S_{dq} = 0.8568%)[24-25].

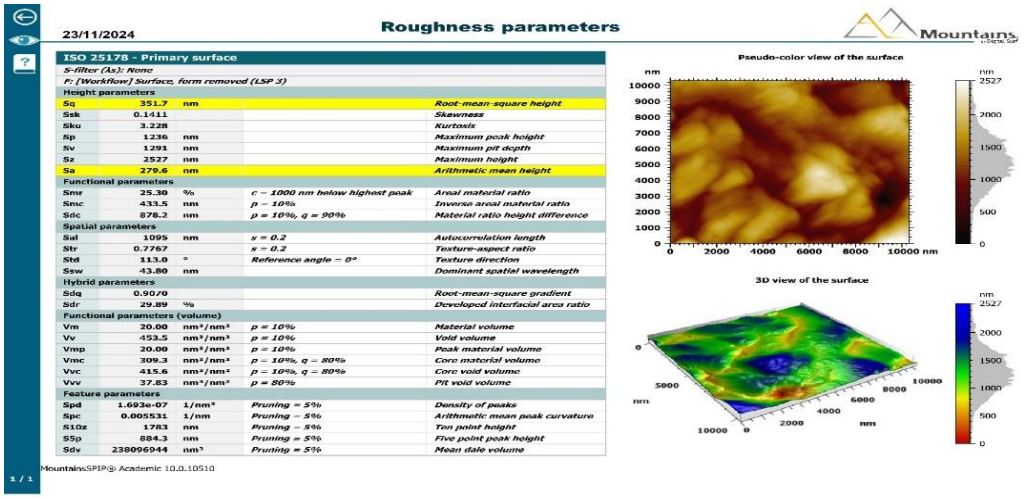

Figure 1. AFM result for the $PbBa_2Ca_2Cu_3O_{9+\delta}$.

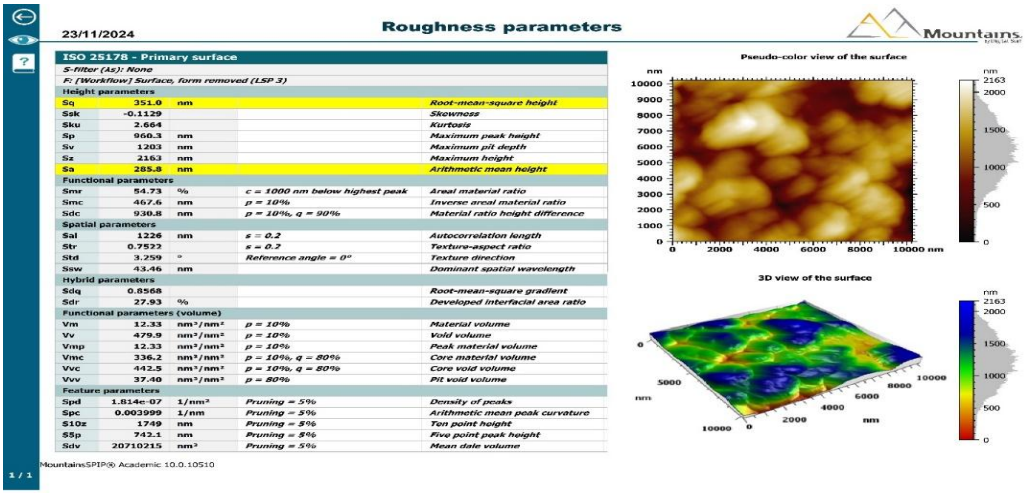

Figure 2. AFM result for the $Pb_{0.85}Cd_{0.15}Ba2Ca2Cu3O9$.

3.2. Critical Temperature

The electrical resistivity of the $Pb_{1-x}Cd_xBa_2Ca_2Cu_3O_{9+\delta}$ combination was measured as a function of temperature using a four-sensor approach to identify crucial transitions. The base sample (x=0) exhibited a sharp decrease in resistivity starting at $T_{c(onset)}$ = 200.25 K and reaching zero at $T_{c(offset)}$ = 147.3 K, as illustrated in **Figure 3**. Upon doping with Cadmium (x=0.15), a general reduction in resistivity was observed, though the transition temperatures decreased marginally to $T_{c(onset)}$ = 198.92$ K and $T_{c(offset)}$ = 146.9 K **Figure 4**[14,26-28].

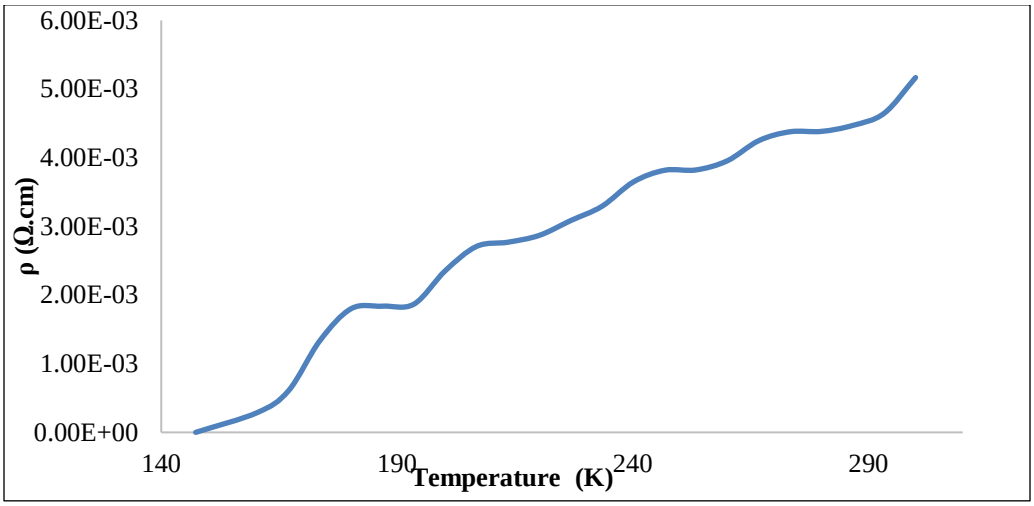

Figure 3. Shows how the resistivity of the $PbBa_2Ca_2Cu_3O_{9+\delta}$ compound changes with temperature at (x = 0.0).

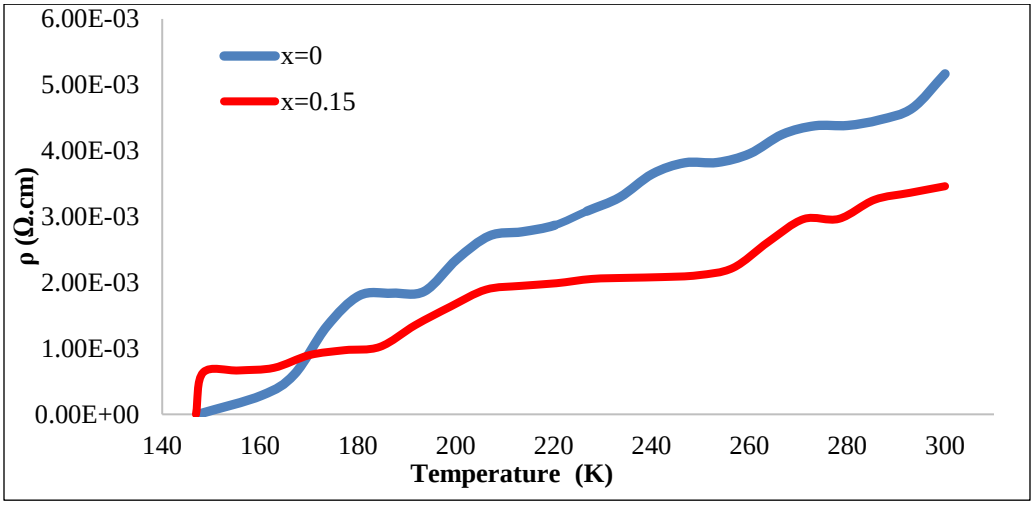

Figure 4. Shows how the resistivity of the $Pb_{1-x}Cd_xBa_2Ca_2Cu_3O_{9+\delta}$ compound changes with temperature at concentration x = 0.0,0.15.

3.3. Dielectric Properties

We used this device (4294A Precision Impedance Analyzer), which quantified capacitance (Cp), Real dielectric constant(έ), and dissipation factor (D) as a function of the applicable frequency, was utilized in the range of 200 KHz-1MHz at room temperature. Frequency-dependent dielectric studies (200 kHz-1 MHz) provided important insights into the polarization dynamics of the material. For the undoped sample (x = 0), the dielectric constant (ε) decreased monotonically with increasing frequency **Figure 5.** Indicating interfacial polarization (Maxwell-Wagner effect) caused by heterogeneous grain boundaries and secondary phases[29-32.] The near-zero ε values at high frequencies (1 MHz) indicate minimal dipolar relaxation, as carriers cannot follow fast field oscillations. Cadmium (Cd) doping (x = 0.15) enhanced this effect, resulting in even lower ε values. This reduction is attributed to the ability of Cd to homogenize the microstructure by suppressing grain boundary defects and secondary phases, resulting in less space charge build-

up[29-32]. The high Cd exchange ratio increases the concentration of charges and holes within the sample, as observed in the dielectric constant values at intermediate frequencies. In addition, the strong bonding and cohesion between elements, enhanced by Cd doping, contribute to the electrical properties of the material, as evidenced by dielectric constant values approaching zero[31]. Significant improvements have been observed in each property, with models showing similar behavior when voltage and current are measured at different frequencies.

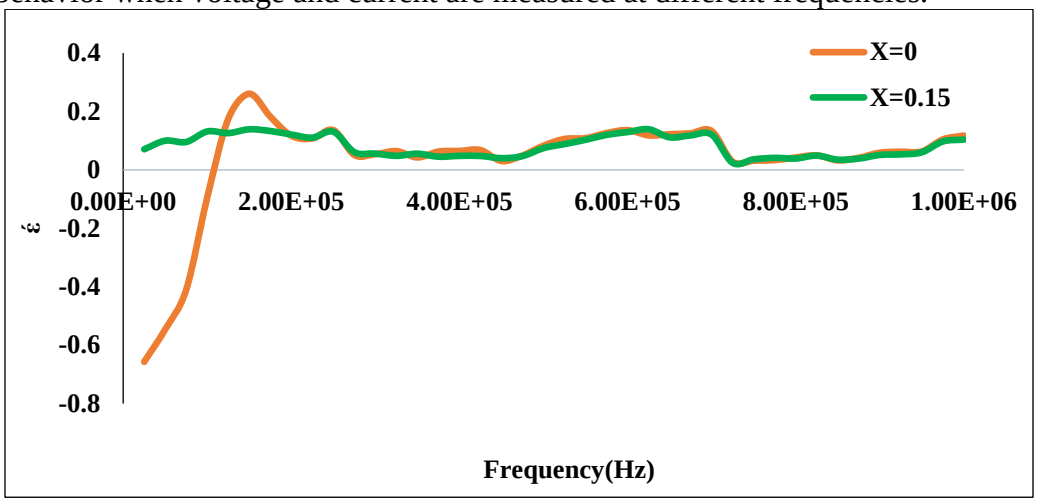

Figure 5. Dielectric constant for the $PbBa_2Ca_2Cu_3O_{9+\delta}$ and $Pb_{0.85}Cd_{0.15}Ba_2Ca_2Cu_3O_9$

Essential insights into the polarization dynamics of the material and the effect of cadmium (Cd) doping were obtained by frequency-dependent dielectric studies in the range 200 kHz to 1 MHz For the undoped sample (x = 0), the imaginary permittivity (ε") and dielectric loss (tan δ) exhibited frequency-dependent peaks **Figures 6** and **7**, indicating relaxation processes such as interfacial polarization caused by heterogeneous grain boundaries and secondary phases. The dielectric constant decreased with increasing frequency, and near-zero ε" values at high frequencies (1 MHz) indicated minimal dipolar relaxation, as carriers could not follow fast field oscillations. For Cd doping at x = 0.15, these peaks broadened and shifted to higher frequencies, indicating that Cd incorporation increases structural cohesion and decreases relaxation time. Cd substitution modifies the crystal structure, resulting in a more stable and uniform lattice by suppressing grain boundary defects and minimizing secondary phases and impurities[29-32]. This structural improvement reduces space charge buildup and defects, contributing to lower dielectric losses at higher frequencies. Kumar and Singh's model[32] supports these observations, postulating that Cd strengthens inter-element bonding, stabilizes the lattice, and minimizes defect-mediated conduction pathways. The strong bonding and cohesion between elements due to Cd doping reduce energy dissipation due to ionic hopping and leakage currents. As the electric field frequency increases, the dielectric loss factor tends to increase due to internal friction and surface or volume leakage currents. However, the Cd-induced improvements result in lower electrical losses at higher frequencies, reflecting improved electrical properties consistent with the polarization dynamics of the material.

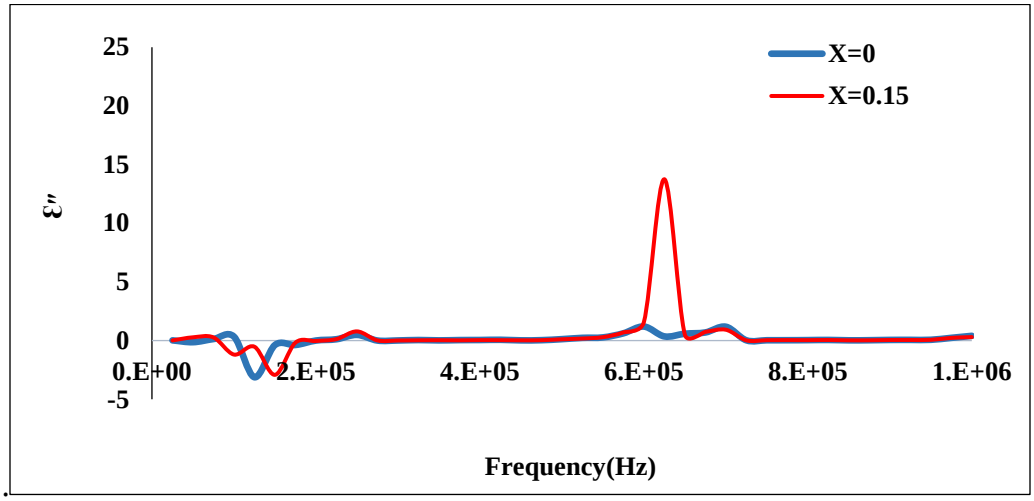

Figure 6. Variations in the imaginary dielectric constant as a function of frequency for the $PbBa_2Ca_2Cu_3O_{9+\delta}$ and $Pb_{0.85}Cd_{0.15}Ba_2Ca_2Cu_3O_9$.

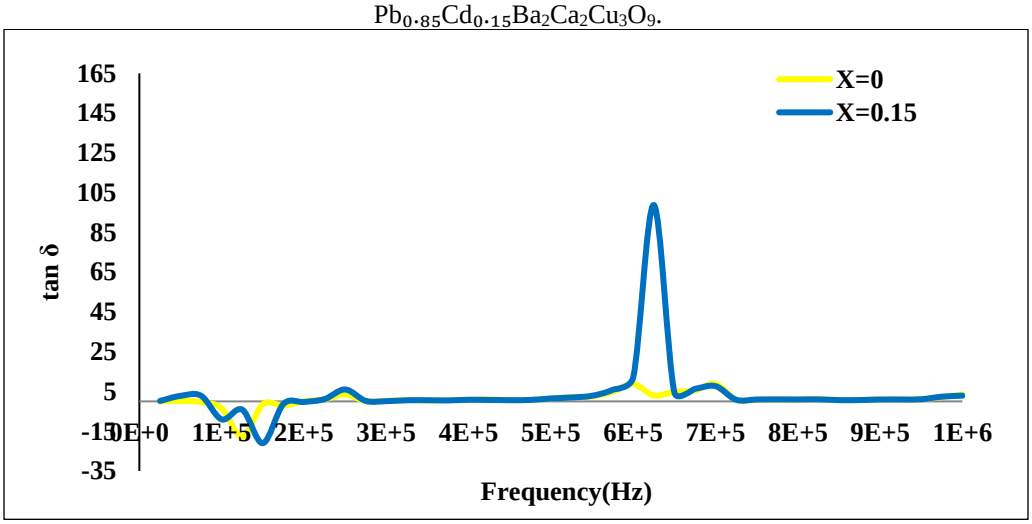

Figure 7. Variations in the dielectric loss factor as a function of frequency for the $PbBa_2Ca_2Cu_3O_{9+\delta}$ and $Pb_{0.85}Cd_{0.15}Ba_2Ca_2Cu_3O_9$.

The power loss is explained by the energy required to maintain rotation, and, conversely, as the frequency increases, the surface and volumetric leakage currents increase, and variations in capacitance can also be directly related to the imaginary dielectric constant. These variations in loss values from sample to sample can be caused by the presence of liquid and impurities as a result of the change in replacement ratio due to the possibility of different heat distribution on the sample within the furnace during the sintering process for one sample, as well as between samples. According to **Equation (4)**[23].

Figure 8 show the relationships between electrical conductivity as a function of frequency, correspondingly part of the energy is received by the electric field, and the alternating conductivity specifies how much insulation is lost as a result of the movement of the dipoles when the dielectric material is exposed to the action of the alternating field, as shown by **Equation (5)**[23] It is important to note that the electrical conductivity in insulators originates from where it can be observed through this relationship the direct dependence of the alternating conductivity on both the frequency of the electric field pointed out and its dependence on the imaginary part of the dielectric constant, which represents the absorption of energy and its dispersion in the insulating material under the influence of an alternating electric field[23]. Various materials have dissimilar dielectric qualities, which are affected by external parameters such as humidity, temperature, crystal structure, applied field frequency, etc. In other words, the answer may be non-linear or linear.

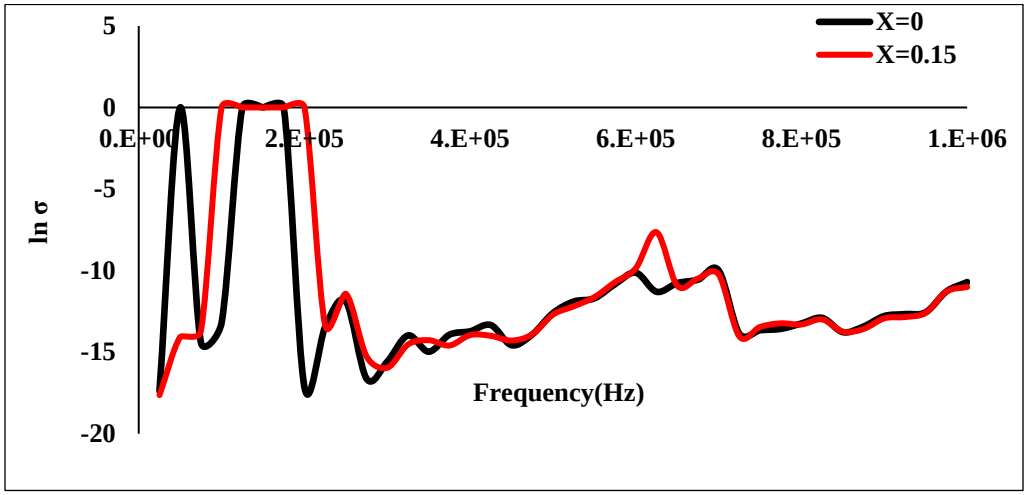

Figure 8. Electrical Conductivity as a function of frequency for the $PbBa_2Ca_2Cu_3O_{9+\delta}$ and $Pb_{0.85}Cd_{0.15}Ba_2Ca_2Cu_3O_9$.

4. Discussion

The comprehensive analysis of the Pb1-xCdxBa2Ca2Cu3O9+ δ material, combining Atomic Force Microscopy (AFM), electrical resistivity, and frequency-dependent dielectric studies, reveals that Cadmium (Cd) doping significantly improves the surface and electrical homogeneity, making the x=0.15 sample superior for superconducting applications. AFM analysis, based on ISO 25178, showed that the doped Sample 2 has a more uniform surface texture with a more balanced peak-valley distribution (lower Sz and Sku) and higher material coverage (Smr), which is critical for minimizing defects in superconductors. Electrically, the base sample (x=0) exhibited a sharp superconducting transition Tc(offset) = 147.3 K), and while Cd doping caused a slight decrease in Tc due to minor lattice distortions, the preserved sharp transition and overall lower resistivity suggest that Cd^{+2} substitution for Pb^{+2} effectively optimizes hole concentration and enhances interlayer coupling within the perovskite structure. Dielectric studies (200 kHz-1 MHz) further supported these findings, where the monotonic decrease in the dielectric constant (έ) and frequency-dependent peaks in imaginary permittivity (ε") and dielectric loss (tan δ) in the undoped sample were primarily due to interfacial polarization (Maxwell-Wagner effect) at heterogeneous grain boundaries. Cd doping strongly diminished this effect by homogenizing the microstructure, suppressing defects, and increasing structural cohesion, which shifted the relaxation peaks to higher frequencies, reduced the dielectric loss (tan δ), and lowered the overall alternating conductivity(σac) loss at high frequencies, confirming a more stable lattice with reduced energy dissipation.

5. Conclusion

Through a comprehensive analysis of AFM results and electrical measurements, it has been observed that the addition of cadmium (Cd) led to significant enhancements in the structural and electrical properties of the material. AFM results showed a significant decrease in surface roughness values (Sa = 285.8 nm) and an increase in material percentage (Smr = 54.73%), indicating enhanced material cohesion and surface distribution. Furthermore, the addition of cadmium improved inter-elemental bonding, resulting in a sharp decrease in electrical resistance to near zero, indicating improved electrical conductivity. In terms of dielectric properties, the results showed that the dielectric constant and dielectric loss factor changes with changes in cadmium content. In general, a decrease in dielectric loss factor leads to an increase in electrical energy absorption, reflecting an improvement in insulation efficiency. The addition of cadmium promotes inter-elemental bonding and reduces crystal defects, leading to improved dielectric properties and reduced dielectric losses, especially at high frequencies. These results confirm that cadmium addition has a positive effect on the structural and electrical properties of the material,

making it a suitable candidate for applications that require improved electrical insulation and high conductivity.

Acknowledgment

We would like to present my deep acknowledgment to the University of Baghdad / College of Engineering / Department of Energy for their support, and the University of Baghdad / College of Education for Pure Science Ibn Al-Haitham / Department of Physics staff for their support in providing analytical tests.

Conflict of Interest

The authors declare that they have no conflicts of interest.

Funding

None.

Ethical Clearance

The project was approved by the local ethical committee at the University of Baghdad.

References

1. Iyo A, Tanaka Y, Kito H, Kodama Y, Shirage PM, Shivagan DD. Watanabe. Condensed matter: Electronic structure and electrical, magnetic, and optical properties vs n Relationship for MultilayeredHigh-Tc Superconductors. J Physics Procedia. 2007;76(9):94711-94711. https://doi.org/10.1143/JPSJ.76.09471
2. Pickard CJ, Errea I, Eremets MI. Superconducting hydrides under pressure. Annu Rev Condens Matter Phys. 2020;11:57–76. https://doi.org/10.1146/annurev-conmatphys-031218-013413
3. Tanaka S. High-temperature superconductivity: historical perspectives. Cham (Switzerland): Springer Nature; 2022.
4. Mangin S, Bellouard C. Superconductivity: from basic physics to applications. Les Ulis (France): EDP Sciences; 2020.
5. Zhou X. High-temperature superconductivity. Nat Rev Methods Primers. 2021;1(1):35. https://doi.org/10.1038/s43586-021-00035-y.
6. Cava RJ. The discovery of high-temperature superconductors. Front Phys. 2019;7:21. https://doi.org/10.3389/fphy.2019.00021
7. Geballe TH, Moyzhes BY. The physics of high-Tc cuprate superconductors. In: Oxford Research Encyclopedia of Physics. Oxford: Oxford University Press; 2021. https://doi.org/10.1093/acrefore/9780190871994.013.149
8. Prozorov R, Giannetta RW. Magnetic Penetration Depth in Unconventional Superconductors. Topical review. Supercond Sci Technol. 2006;19(8): R41. https://doi.org/10.1002/chin.200702273
9. Cardoso CA, Araujo-Moreira FM, Awana VPS, Kishan H, Takayama-Muromachi E, de Lima OF. Magnetic properties of the $RuSr_2Ln_{1.5}Ce_{0.5}Cu_2O_{10-}\delta$ (Ln=Y, Ho, Dy) and $RuSr_2YCu_2O_{8-}\delta$ rutheno-cuprate families. Physica C. 2004;405(3–4):212. https://doi.org/10.1016/j.physc.2004.02.012
10. Wu J, Lee S. Next-generation high-temperature superconductors: synthesis and electronic characterization. Prog Mater Sci.2024; 142:101235.https://doi.org/10.1016/j.pmatsci.2023.101235
11. West AR. Solid state chemistry and its applications. 2nd ed. Hoboken (NJ): John Wiley & Sons; 2020.
12. Khalid M. Recent advances in high-temperature superconductors: materials, properties and applications.2023;16(2):541. https://doi.org/10.3390/ma16020541.
13. Hirsch JE, Marsiglio F. The evolution of superconductivity: from 1911 to the present. Physica C Supercond Appl. 2022; 600:1354079. https://doi.org/10.1016/j.physc.2022.1354079
14. Jasim KA, Mohammed LA. The partial substitution of copper with nickel oxide on the structural and electrical properties of $HgBa_2Ca_2Cu_{3-x}Ni_xO_{8+}\delta$ superconducting compound. J Phys Conf Ser. 2018;1003:012071. https://doi.org/10.1088/1742-6596/1003/1/012071
15. Nurbaisyatul ES, Azhan H, Kasim A, Ibrahim N. Effect of $\{CeO\}^{-2}$ Nanoparticle on the Structural and Electrical Properties of BSCCO-2223 High Temperature Superconductor. Solid State Phenom. 2020; 307:104–9.

16. Maqsood, A. and Maqsood, M., 1996. Proceeding of the international workshop held at Rajshahi University, Bangladesh, 28 Oct-1 Nov. Edited by AKMA Islam.
17. Ghahfarokhi SEM, Hoseenzadeh N, Shoushtari MZ. The Effect of CdO Nanoparticles on the Structure and Magnetic Properties of Bi 1. 6 4 Pb 0. 3 6 Sr 2 Ca 2 − x Cd x Cu 3 O y Superconductors. J Supercond Novel Magn. 2014;27(10):2217–2223.
18. Kittel C. Introduction to solid state physics. 7th ed. California: [Publisher Name, typically Wiley]; 2004. p. 17.
19. Rose AC, Rhoderick EH. Introduction to superconductivity. Oxford (UK): Pergamon Press; 1976.
20. Ford PJ, Saunders GA. High temperature superconductors: ten years on. Phys J. 1997;38(1):63.
21. Kalsi SS. Superconducting wind turbine generator employing MgB_2 windings both on rotor and stator. IEEE Trans Appl Supercond. 2014;24(1):5201907.
22. Mumtaz M, Khan NA, Khan S. Study of dielectric properties of oxygen-postannealed $Cu_{0.5}Ti_{0.5}Ba_2Ca_2(Cu_{3-\gamma}M_\gamma)O_{10-}\delta$ superconductor. IEEE Trans Appl Supercond. 2013;23(2):1–8.
23. Tawfiq LNM, Hassan MA. Estimate the effect of rainwaters in contaminated soil by using Simulink technique. J Phys Conf Ser. 2018;1003:012057.
24. ISO 25178:2016. Geometrical product specifications (GPS) — Surface texture: Areal.
25. Farman SA, Ibrahim MK, Aadim KA. The impact of nanomaterials on fabrication silicon solar cells by pulsed laser deposition. NHC. 2020;30:41–54.
26. Maher AH, Jasim KA, Hussein AM. Synthesis and comparative analysis of crystallite size and lattice strain of $Pb_2Ba_{1.7}Sr_{0.3}Ca_2Cu_3O_{10+}\delta$ superconductor. Korean J Mater Res. 2022;32(2):12–23. https://doi.org/10.3740/MRSK.2022.32.2.66
27. van der Haar M. Mixed-conducting perovskite membranes for oxygen separation [Doctoral Thesis]. Enschede (Netherlands): University of Twente; 2001.
28. Hamadneh IK, Hui YW, Abd-Shukor R. Formation of $Tl_{0.85}Cr_{0.15}Sr_2CaCu_2O_{7-}\delta$ superconductor from ultrafine co-precipitated powders. Mater Lett. 2006;60(6):734–6.
29. Mohammed, N.H. Effect of MgO Nano-oxide Additions on the Superconductivity and Dielectric Properties of $Cu_{0.25}Tl_{0.75}Ba_2Ca_3Cu_4O_{12-\delta}$ Superconducting Phase. J Supercond Nov Magn. 2012; 25, 45–53. https://doi.org/10.1007/s10948-011-1207-4.
30. Anderson PW. Spin-charge Separation is the Key to the High-T_c Cuprates. Physica C Supercond. 2000; (9–10):341–348.
31. Choudhary R, Palai R, Sharma S. Structural, dielectric and electrical properties of lead cadmium tungstate ceramics. Mater Sci Eng B. 2000;77(3):235–40.
32. Kumar AS, Babu PD, Srinath S. Magnetization and neutron diffraction studies on nanocrystalline tetragonal $SrFeO_{3-}\delta$. J Supercond Nov Magn. 2017;30(11):3155–9. https://doi.org/10.1007/s10948-017-4125-2